

EFFECT OF REINFORCEMENT ON STRUCTURAL AND OPTICAL PARAMETERS OF POLY (3-HYDROXYBUTYRATE-co-10 MOL% 3HYDROXYHEXONATE)/ZnO COMPOSITES

V. C. JANAKIRAMAN, S. SHANMUGAN*, D. MUTHARASU, A. A. AZLAN
School of Physics, Universiti Sains Malaysia (USM), 11800, Minden, Pulau Pinang, Malaysia

Using solution casting method, virgin poly(3-hydroxybutyrate-co-10 mol% 3hydroxyhexonate) (P(3HB-co-10 mol% 3HHx)) copolymer and ZnO nano particles (NPs) reinforced P(3HB-co-10 mol% 3HHx) composite films were prepared and their structural and optical parameters were studied using X-Ray Diffraction (XRD), Atomic Force Microscopy (AFM) and UV-Vis Spectroscopy. The crystallinity of the prepared composites were decreased due to the addition of ZnO NPs except for 20% ZnO concentration where the crystallinity of the composite is higher than the virgin P(3HB-co-10 mol% 3HHx) copolymer. The crystallite size of the composites is high (311 nm) compared to virgin P(3HB-co-10 mol% 3HHx) copolymer (33 nm) and the dislocation density was decreased with respect to the P(3HB-co-10 mol% 3HHx) crystal orientations. With respect to the concentration of ZnO NPs and P(3HB-co-10 mol% 3HHx) copolymer, the structural properties of the ZnO NPs in the copolymer matrix were also affected noticeably which was confirmed through AFM. Texture coefficient analysis confirms that addition of ZnO NPs in the copolymer matrix changes the preferential orientation of P(3HB-co-10 mol% 3HHx) copolymer which was observed in XRD. UV-Vis spectroscopy studies reveals that ZnO NPs increased the absorbance behaviour of P(3HB-co-10 mol% 3HHx) copolymer in UV-B and UV-C region and decreased the absorbance (high reflection) in visible region (800 nm to 1000 nm) i.e. transmittance behaviour increased which was confirmed in the reflectance and transmittance spectra. Even though the addition of ZnO NPs decreased the crystallinity on the other hand increased the absorption in UV region. From these observations, ZnO NPs reinforced P(3HB-co-10 mol% 3HHx) composites may be used as a UV-blocker or visible reflector for optoelectronics applications.

(Received June 11, 2018; Accepted October 10, 2018)

Keywords: P(3HB), 3HHx, ZnO nanoparticles, Composites, XRD, AFM, UV-Vis

1. Introduction

The growth and usage of non-biodegradable petroleum based plastics have increased drastically which in turn increases the ecological contamination across the entire planet [1, 2]. The petroleum based plastics like polypropylene, polystyrene, polyethylene and polyvinyl chloride are currently considered as very important materials and used in most of the manufacturing industries ranging from consumer products, medical to automobiles due to their easy structural modification properties. The structure and properties of plastics can be easily manipulated chemically to have wide range of applications [3-5]. The main disadvantages in the petroleum-based plastics are its non-biodegradable nature and difficulty in disposal and recycle which makes them undesirable [2, 3, 6]. Being xenobiotic, petroleum based synthetic plastics are intractable to enzymatic degradation [6]. The increased accumulation of synthetic plastics which contains highly contaminated particles requires high energy, cost and takes huge time to recycle or dispose [2, 3, 7]. This growing threat to the ecosystem has given impetus to many developed countries to develop a renewable and bio-degradable material that can replace the existing non-biodegradable synthetic plastics in order to reduce the pollution in the environment [3, 8-10]. The material that

*Corresponding author: subashanmugan@gmail.com

can be degraded and disintegrated by the enzymatic actions of living organisms such as bacteria, fungi and yeast is termed as biodegradable materials [11]. Chemically synthesized polymers, starch-based plastics, and biologically synthesized polymers such as polyhydroxyalkanoates (PHA) are the three categories in biodegradable plastics [12], in which PHA is the only 100% biodegradable material developed from renewable sources [13, 14]. PHA is biotechnological polyester synthesized by bacteria in the intercellular region (i.e. cytoplasm) in the form of carbon and oxygen [15]. It exhibits properties which are similar to non-biodegradable thermoplastics such as polypropylene [16] or elastomers with melting point ranging from 40 °C to 180 °C, and hence can be used as a substitute for thermoplastics and elastomers [1,12,17].

Poly(3-hydroxybutyrate) [P(3HB)] is the first homopolymer to be discovered from PHA [18] which belong to the aliphatic polyester family and can be considered as natural and renewable thermoplastic [19]. It is produced by bacterial fermentation method and is widely gaining attention in biomedical and food processing industry due to its biodegradable and biocompatible nature [19, 20]. Though it is biodegradable, biocompatible and UV absorbable, P(3HB) still couldn't extend its range of applications in the industry due to these main drawbacks such as brittleness, stiffness, rigidity, high production cost. In order to improve the flexibility and decrease the brittleness, different monomer units will be copolymerized with P(3HB) homopolymer [21]. In this case, 3HHx monomer units is copolymerized with P(3HB) homopolymer which results in formation of poly(3-hydroxybutyrate-co-3-hydroxyhexanoate) [P(3HB-co-3HHx)] copolymer. In order to overcome these drawbacks and to extend its range of applications another approach has been reported where P(3HB) was mixed with polyethylene oxide, polycaprolactone, polylactide, polyvinyl alcohol [22]. Another approach being polymer nanocomposites, which exhibits exceptional properties compared to pure polymers and traditional composites [23]. Adding nanofillers such as hydroxyapatite [24], organically modified montmorillonite (OMMT) [25], and multi-walled carbon nanotubes [26] into the polymer matrix will modify the polymer structure, which may improve the physical, optical, thermal properties of the polymer. Noble metal oxide nanoparticles has drawn great attention among researchers due to its unique properties, especially because of low cost, uv absorption, heat barrier, thermal conductivity, antibacterial properties, nanostructured ZnO plays a vital role in electronics, optoelectronic applications, space applications, food and packaging application [27-29]

Yu et al. [30] and Díez-Pascual et al. [31] reported about the preparation of poly(3-hydroxybutyrate-co-3-hydroxyvalerate) [(PHBV)] / ZnO NPs composite and PHB/ZnO NPs composite by electrospinning and solution casting method respectively. Yu et al. stated that ZnO NPs acts as a retarding agent that decreases the degree of crystallization and rate of crystallization in his work whereas Díez-Pascual et al. reported that ZnO NPs acts as a nucleating agent that increases the degree of crystallinity. However, there is no previous work reported involving the detailed structural analysis of ZnO NPs and biodegradable P(3HB-co-10 mol% 3HHx) copolymer. In order to study the effect of ZnO NPs on the structural, UV absorption behaviour and surface properties of P(3HB-co-10 mol% 3HHx) copolymer, six different concentrations of ZnO NPs were reinforced with P(3HB-co-10 mol% 3HHx) copolymer and characterized using X-Ray Diffraction (XRD), UV-Vis spectroscopy (UV-Vis) and Atomic Force Microscopy (AFM). In this study, in addition to peak position and peak intensity analysis, other important XRD parameters such as crystallite size, dislocation density and texture coefficient analysis and the influence of P(3HB-co-10 mol% 3HHx) copolymer on the ZnO's crystallinity were also discussed in detail.

2. Experimental details

2.1 Biosynthesis and extraction of P(3HB-co-10 mol% 3HHx) copolymer by recombinant *C. necator* Re2058/pCB113

Two loopfuls of recombinant *C. necator* Re2058/pCB113 cells were cultured in nutrient rich (NR) agar plates for 24 hours and transferred to NR broth which was then incubated at 30 °C for 8 hours. 100 mL minimal medium were prepared in a shake flask that contains 2 gL⁻¹ of palm olein, 7 gL⁻¹ of fructose and 0.54 gL⁻¹ of urea. These cultured cells were inoculated into the minimal medium and used as inoculum for the fermenter. The fermenter is equipped with control

systems for dissolved oxygen [INFORS HT (Labfors 3), Switzerland], pH, and temperature. The temperature of the culture medium was maintained at 30 °C constantly. Through controlled addition of 3M sodium hydroxide and 3 M phosphoric acid, the pH of the culture medium was maintained at 7.0 ± 0.1 . Three sic blade Rushton impeller operating at a speed of 200-900 rpm and 1 VVM air was supplied through filter cartridges (Sartorius stedim, Germany) and the dissolved oxygen concentration was maintained at above 40%. Autoclave (HV110, Hiriyama, Japan) was used to sterilize the culture medium together with fermenter at 121 °C for 30 minutes. In order to extract the polymer, freeze dried cells were mixed in chloroform with the ratio of 1 g: 100 mL and stirring was continued for 5 days at room temperature. The resulting solution was filtered to remove the cell debris and then the filtered solution was concentrated by using a rotary evaporator. To extract the polymer, the concentrated solution was added drop-wise into vigorously stirred chilled methanol for 1 h to precipitate and purify. The extracted and purified polymer was then used for experiments.

2.2 Preparation of virgin copolymer and ZnO NPs filled composite film

Extracted and purified P(3HB-co-10 mol% 3HHx) copolymer (500 – 350 mg) was dissolved in chloroform solvent together with 6 different concentration of ZnO NPs ranging from 5 % to 30% (25 - 150 mg) and stirred using mechanical stirrer until a colloidal solution was obtained and then the colloidal solution was sonicated for 30 min. Then the solution was casted in petri dish with 55 mm diameter at room temperature for 48hours. After 48 hrs, the film was retrieved from the petridish and thickness was measured. The measured film thickness was 0.3 mm with diameter of about 50mm. The sample name throughout this manuscript is given based on the information provided in Table 1. Hereafter, the short form will be used for discussion.

Table 1. Sample Information and Naming.

Sample composition	Total weight = weight of Poly[3-hydroxybutyrate-co-15 mol% 3hydroxyhexonate] copolymer + ZnO nanoparticles	Name of the sample
Poly[3-hydroxybutyrate-co-10 mol% 3hydroxyhexonate P(3HB-co-10 mol% 3HHx)	500 mg	PHB-10HZ0
P(3HB-co-10 mol% 3HHx) + 5% ZnO	475 mg + 25mg	PHB-10HZ5
P(3HB-co-10 mol% 3HHx) + 10% ZnO	450 mg + 50mg	PHB-10HZ10
P(3HB-co-10 mol% 3HHx) + 15% ZnO	425mg + 75 mg	PHB-10HZ15
P(3HB-co-10 mol% 3HHx) + 20% ZnO	400mg + 100mg	PHB-10HZ20
P(3HB-co-10 mol% 3HHx) + 25% ZnO	375 mg + 125 mg	PHB-10HZ25
P(3HB-co-10 mol% 3HHx) + 30% ZnO	350mg + 150mg	PHB-10HZ30

2.3. X-Ray Diffraction (XRD)

The D8 Bruker X-ray diffractometer (Model: PANalytical X'Pert PRO MRD PW3040) with Cu-K α radiation (wavelength = 1.5406 Å) beam operated at 40 kV and 40 mA was used to investigate the structural properties of virgin PHB-10HZ0 copolymer and ZnO NPs reinforced PHB-10HZ0 composite films. The effect of different concentrations of ZnO NPs on the crystallinity and amorphous behaviour of PHB-10HZ0 copolymer and the effect of PHB-10HZ0 copolymer on the ZnO NPs crystallinity behaviour was studied. The X-ray diffraction spectra were captured for all the samples in the scan range from $2\theta = 10^\circ$ to 90° under continuous mode using the scan step rate of 0.02° with scan step time of 190 seconds. The peaks were indexed using the X'Pert Score software and compared with the results published in literature and JCPDS file.

2.4 UV Vis spectrophotometer

In order to analyze the optical properties of virgin PHB-10HZ0 copolymer and ZnO reinforced PHB-10HZ0 composites, the UV-Vis spectrophotometer (Shimadzu UV-Vis 1800) was used to record the absorbance and transmission spectra for the wavelength range from 200 to 1000 nm.

2.5 Atomic force microscopy (AFM)

The surface topography of virgin PHB-10HZ0 copolymer and ZnO reinforced PHB-10HZ0 composite film samples were captured by AFM (Model: Dimension EDGE, BRUKER) using tapping mode. Nanoscope analysis software was used to evaluate the surface roughness and particle size of all samples.

3. Results and discussion

3.1 XRD characterization

3.1.1. Peak analysis

In order to study the crystalline and amorphous behaviour of PHB-10HZ0 copolymer, XRD spectrum for all the prepared samples with different ZnO NPs concentrations were taken and plotted in graph as shown in Fig. 1. From the Fig. 1, several important characteristics peaks were identified and indexed to PHB-10HZ0 copolymer and ZnO NPs. The identified PHB-10HZ0 copolymer peaks (2θ) were 13.52° , 16.96° , 20.07° , 21.85° , 22.34° , 25.61° , 27.16° , 29.39° are almost identical with that published results [32-38]. The peaks observed at $2\theta = 13.52^\circ$, 16.96° , 20.07° , 21.85° , 22.34° , 25.61° , 27.16° , 29.39° correspond to the (020), (110), (021), (101), (111), (121), (040) and (002) reflections which were identified as orthorhombic crystalline lattice related to polymer [36, 38, 39]. The following peaks (2θ) observed at 31.84° , 34.52° , 36.39° , 47.69° , 56.75° , 63° , 66.51° , 68.09° , 69.23° , 72.7° , 81.51° and 89.73° are indexed to ZnO NPs and verified with JCPDS file nos. 790205 and 897102.

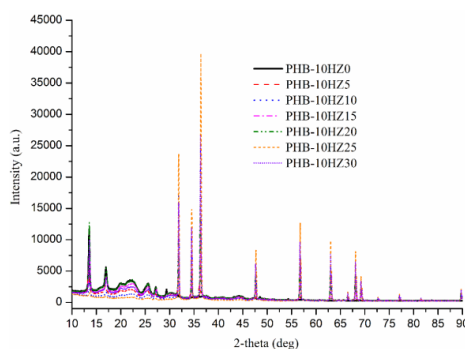


Fig. 1. Complete XRD spectra of PHB-10HZ0 copolymer and ZnO NPs in PHB-10HZ0/ZnO NPs composites.

The change in peak intensity changes of virgin PHB-10HZ0 copolymer and PHB-10HZ0/ZnO NPs composites at characteristic peak 13.52° (020) is shown in Fig. 2a. The influence of ZnO NPs in the intensity changes i.e. crystalline and amorphous behavior of the characteristic PHB-10HZ0 polymer peak (13.52°) is analyzed here. From the Fig. 2a, it clearly picturizes that the PHB-10HZ20 sample shows high intensity than virgin PHB-10HZ0 copolymer and its composites which indicates that PHB-10HZ20 is highly crystalline and pure when compared to virgin PHB-10HZ0 copolymer and its composites. This increased intensity showed that the PHB-10HZ20 composite may have more organized packed crystalline structure [40]. Except PHB-10HZ20, PHB-10HZ0 shows high intensity than all other composite samples which clearly indicates that ZnO NPs increases the amorphous behavior of PHB-10HZ0 copolymer. 20% ZnO NPs concentration acts as a nucleating agent, whereas other concentrations act as a retarding agent for PHB-10HZ0 copolymer. Rithin kumar et al [41] have reported that the decrease in crystalline behavior is may be due to the molecular interaction between the PHB-10HZ0 copolymer and ZnO NPs which in turn decreases the intermolecular interaction between the chains formulated in PHB-10HZ0 copolymer. In addition to that, as the concentration of ZnO NPs increases, the crystalline behavior of the PHB-10HZ0/ZnO NPs composite samples are not decreasing gradually.

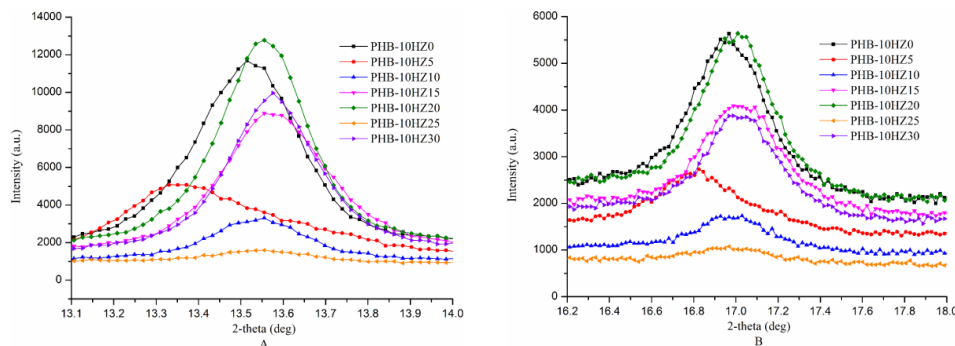


Fig. 2. Variation in peak intensity as well as peak shifting for the XRD spectra of the characteristic peak of PHB-10HZ0 copolymer observed (a) at 13.52° and (b) at 16.96° for different ZnO NPs concentrations.

There is some fluctuation in the decreasing order in which PHB-15HZ20 is followed by PHB-10HZ30 and PHB-10HZ15, PHB-10HZ5, PHB-10HZ10 and PHB-10HZ25 respectively. In general, peak shifts are an indication of crystalline defects and also observed in our PHB-10HZ0/ZnO NPs composite results. It is attributed to the abundant long side chains of the polymer, the existence of different units and their irregular array which affects the crystallinity of the polymer [42] and thus results in amorphous nature. From Fig. 2a, compared to virgin PHB-10HZ0 copolymer sample (13.51°), there is a noticeable peak shift in the higher 2θ is observed for all the composites except PHB-10HZ5 (13.35°) which exhibit peak shift towards lower 2θ .

On considering the characteristic peak 16.96° (110) shown in Fig. 2b, the high intensity peak is observed for PHB-10HZ20 composite sample rather than virgin PHB-10HZ0 copolymer which indicates that crystallinity increases due to the addition of ZnO NPs for this particular concentration (20% ZnO NPs) whereas the crystallinity decreases for all other concentration. Like the previous peak 13.52° , the same trend has been observed for this peak too except the intensity decreasing order.

As considered the three characteristic peaks of PHB-10HZ0 copolymer shown in fig. 3 observed at 20.07° (021), 21.85° (101) and 22.34° (111), the peak intensity of virgin PHB-15HZ0 copolymer and PHB-15HZ20 composite are same. In this area, very broad peaks were observed for all the samples and their intensities were diminishing with the increasing ZnO NPs concentration and with intensity barely observed for PHB-10HZ25 sample. The broad peak indicates that the polymer attains a nano crystalline behavior. As noticed in peak 16.96° , the same decreasing order has been prevailed for all these peaks too.

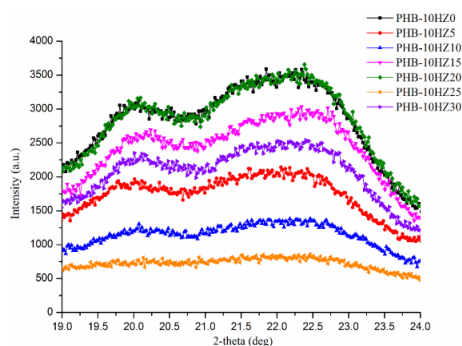


Fig. 3. Effect of different ZnO NPs concentrations on the intensity changes of the characteristic peaks of PHB-10HZ0 copolymer observed at 20.07° , 21.85° and 22.34° .

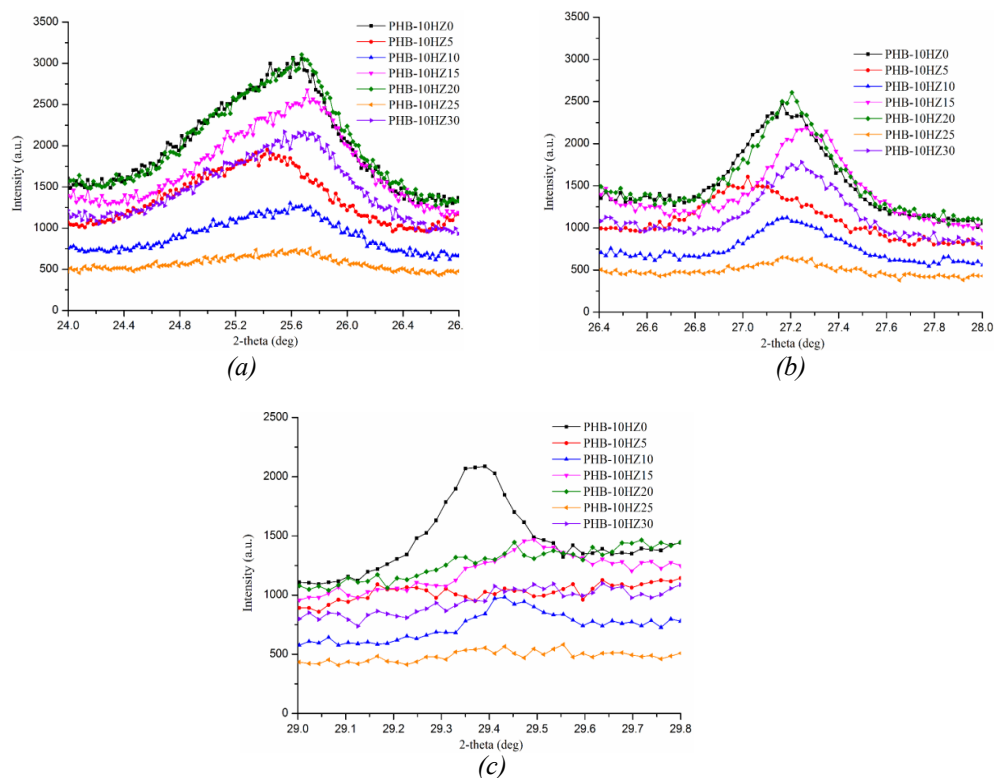


Fig. 4. Change in intensity with respect to various ZnO NPs concentration for the PHB-10HZ0 copolymer peaks observed (a) at 25.61°, (b) at 27.16° and (c) at 29.39°.

The change in intensity with respect to various ZnO NPs concentration for the PHB-10HZ0 copolymer peaks observed at 25.61° (121), 27.16° (040), 29.39° (002) is shown in Fig. 4. On considering the 121 and 040 reflections, PHB-10HZ20 exhibit high intensity than virgin copolymer however the intensity difference is not significant. Apart from that, there is no significant difference between these two peaks and the previously analyzed peaks but for the peak 29.39° (Fig. 4c), only PHB-10HZ0 copolymer sample has been observed with some intensity, all other composites show very broad peaks with small peak shifts towards higher and lower 2θ .

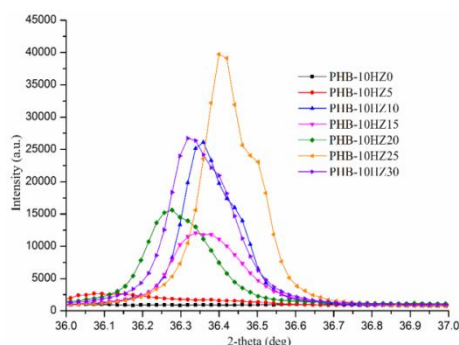


Fig. 5. The XRD spectra of ZnO NPs observed at 36.39° after reinforcing with the PHB-10HZ0 copolymer for various ZnO NP concentrations.

In order to study the effect of PHB-10HZ0 copolymer on the crystallinity behavior of the ZnO NPs, the peak intensity analysis of ZnO NPs is also considered and analyzed in this paper. The peaks with noticeable high intensity which are related to (101), (100), (002), (102), (110),

(103) and (112) orientations are considered here for the analysis (JCPDS – 790205). Fig. 5 shows the intensity changes of (101) oriented peak of ZnO NPs which clearly indicates the presence of ZnO NPs in the PHB-10HZ0 copolymer matrix. PHB-10HZ25 exhibit a very high intensity peak compared to virgin PHB-10HZ0 copolymer and other composites, whereas it exhibits a very low intensity peak in all the polymer-oriented phases. In addition to that, as the ZnO NPs concentration increases, overall the peak intensity of the composites is not increasing gradually in a linear manner which clearly indicates the role of PHB-10HZ0 copolymer in the influence of structural behavior of ZnO NPs. The intensity of (101) oriented ZnO NPs peak is decreasing in the sequence of PHB-10HZ25, PHB-15HZ30, PHB-15HZ10, PHB-15HZ20, PHB-15HZ15, and PHB-15HZ5. The last three samples attain a broader peak with less intensity whereas the first 3 samples attain a very narrow peak with high intensity. There is some distortion in the crystal structure based on the concentration of PHB-10HZ0 copolymer and ZnO NPs which may be attributed to the random changes in the peak intensity [807]. Like polymer peak shifts, (101) oriented peak also attains a major peak shift toward lower 2θ and is observed for all the composites (Fig. 5). This peak shift may be due to a chemical reaction that might change the stoichiometry locally or internal strain that attribute to local structural modification or it may be assigned to the stacking fault in composite structure [43].

On considering the (100) and (002) oriented peak (see Fig. 6), PHB-10HZ25 exhibit high intensity than virgin PHB-10HZ0 copolymer and other composites which indicates that PHB-10HZ25 exhibit high crystallinity followed by other composites in random decreasing order like the previous (101) oriented phase observed at 36.39° . A small peak shift towards lower 2θ is observed for the PHB-10HZ20 and PHB-10HZ5 composite samples whereas PHB-10HZ10 and PHB-10HZ15 attains a small peak shift towards higher 2θ due to the structural distortion and modification as a result of chemical reaction between PHB-10HZ0 copolymer, and ZnO NPs. [44].

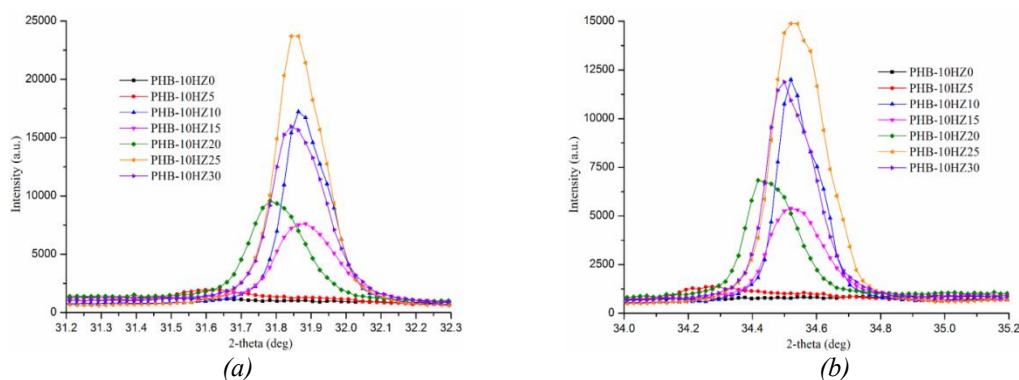


Fig. 6. Variation in peak intensity as well as peak shifting for the characteristic XRD peak of ZnO NPs observed (a) at 31.84° and (b) at 34.52° for various ZnO NPs concentrations.

Fig. 7 shows the characteristic peak of ZnO NPs observed at 47.69° (102) and 56.75° (110), in which the crystallinity of the ZnO NPs increases with increases of ZnO NPs i.e. high intensity is observed for PHB-10HZ25 with a small shoulder peak located besides the above-mentioned peaks followed by other composites. There is a small peak shift towards lower 2θ is observed for PHB-10HZ30, PHB-10HZ20, PHB-10HZ15 and PHB-10HZ5 samples. The following peaks 63° , 68.09° are assigned to (103) and (112) phase respectively as shown in Fig. 8. Like previously explained phase (Fig. 7), these ((103) and (112)) phases also followed the same trend except some changes in the peak intensity.

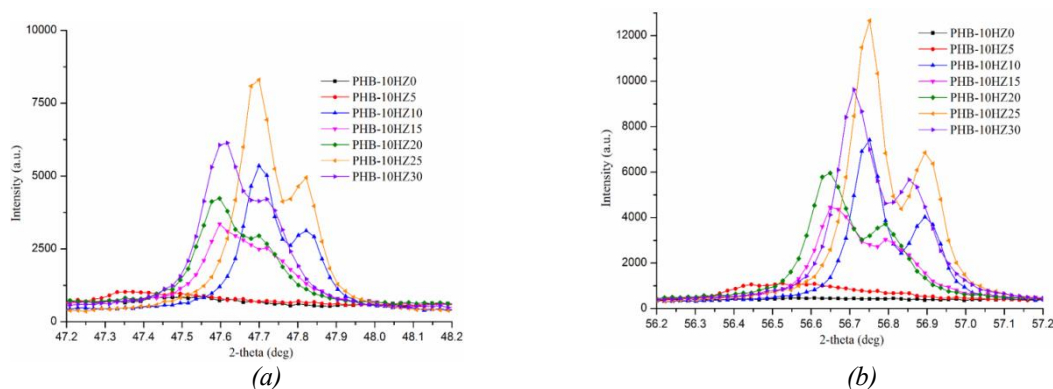


Fig. 7. Change in peak intensity as well as peak shifting for the characteristic XRD peak of ZnO NPs observed (a) at 47.69° and (b) at 56.75° for various ZnO NPs concentrations.

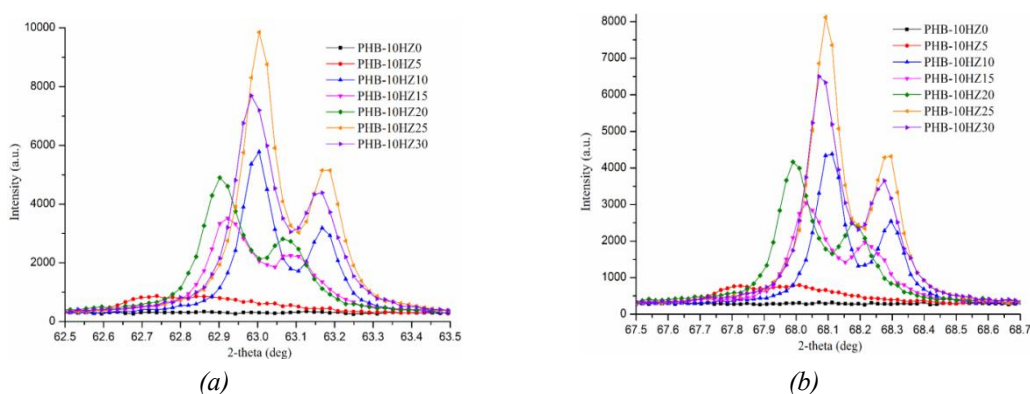


Fig. 8. Variation in peak intensity for the characteristic XRD peak of ZnO NPs observed (a) at 63° and (b) at 68.09°.

3.1.2 Crystallite size analysis

X-ray diffraction technique is the most convenient method to determine the crystallite size of the nanocrystalline material. Virgin PHB-10HZ0 copolymer and ZnO reinforced PHB-10HZ0 composites were analysed to find the crystallite size (D) of PHB-10HZ0 copolymer and ZnO NPs using the Debye-Scherrer equation [25].

$$D = k\lambda/(\beta_D \cos \theta) \quad (1)$$

Where D is the crystallite size in nanometer, k is a shape factor constant equal to 0.94 which is related to crystallite shape, λ is the wavelength of the radiation (1.5406 nm for Cu-K α radiation), β_D is the peak width (i.e. broadening) of diffraction peak measured at half of its maximum intensity (FWHM) and θ is the peak position respectively. The following peaks 13.52°, 16.96°, 20.07°, 22.34°, 25.61°, 27.16°, 29.39° belongs to the PHB-10HZ0 copolymer were considered for the crystallite size analysis. Coming to ZnO NPs, the following peaks 31.84°, 34.52°, 36.39°, 47.69°, 56.75°, 63.01°, 68.09° were considered for crystallite size analysis. The broadening of the peak is a combination of both instrumental errors and other sample dependent defects. In order to avoid these errors, we have considered the instrumental error while calculating the peak width (β_D). It is necessary to correct the instrumental error before determining the crystallite size. Si (111) XRD spectrum was recorded to estimate the instrumental broadening. The corrected broadening (i.e. considering the estimated instrumental broadening) was determined using the following equation [25].

$$\beta_D^2 = [(\beta_D^2)_{\text{measured}} - (\beta^2)_{\text{instrumental}}] \quad (2)$$

The crystallite size of the PHB-10HZ0 copolymer and ZnO NPs in the polymer composites was estimated using the above equation and the obtained results are plotted as shown in Fig. 9.

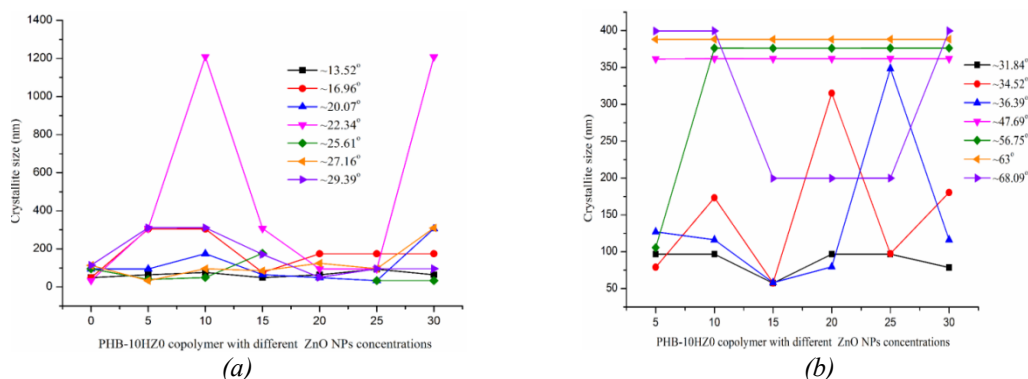


Fig. 9. a) Change in crystallize size of PHB-10HZ0 copolymer in PHB-10HZ0/ZnO NPs composite with respect to different ZnO NPs concentrations, b) change in crystallite size of ZnO NPs in PHB-10HZ0/ZnO NPs composite with respect to different ZnO NPs concentrations.

Fig. 9a & 9b shows the change in the crystallite size of the PHB-10HZ0 copolymer and ZnO NPs vs. different ZnO NPs concentration in the PHB-10HZ0 copolymer which gives the information about the effect of addition of ZnO NPs on the crystallite size of PHB-10HZ0 copolymer and vice versa. The observed crystallite size of PHB-10HZ0 copolymer and ZnO NPs are in nanoscale. From the Fig. 9a & 9b, it clearly indicates that the crystallite size is not increasing gradually as linear but in random manner, and there is some fluctuation in the crystallite size of PHB-10HZ0 copolymer as the concentration of ZnO NPs increases which clearly shows the influence of ZnO NPs in the growth of PHB-10HZ0 copolymer's crystal. Virgin PHB-10HZ0 copolymer was observed with low crystallite size (33 nm) and PHB-10HZ10 and PHB-10HZ30 composite samples were observed with very high crystallite size (1208 nm & 1207 nm). Compared to highest crystallite size that was mentioned above, the next high average crystal size which was around 307 nm was observed for PHB-10HZ5, PHB-10HZ10, PHB-10HZ15 and PHB-10HZ30 composite samples. We eliminated PHB-10HZ20 composite sample's crystallite size value observed at 25.61°, since the FWHM of the observed peak was less than the instrumental error value (0.072°) and hence getting error values in crystallite size calculation. Overall, compared to virgin PHB-10HZ0 copolymer's, crystallite size of PHB-10HZ0 copolymer is high in the presence of ZnO NPs reinforced PHB-10HZ0 composite samples. Figure 9b shows the change in crystallite size of ZnO NPs in PHB-10HZ0 composites with respect to different ZnO NPs concentration. From the Fig. 9b, PHB-10HZ15 composite sample was observed with very small crystallite size with average value around 57 nm whereas PHB-10HZ5, PHB-10HZ10, PHB-10HZ30 composite sample's average crystallite size was around 399 nm which is very high compared to other composite samples. The average crystallite size of all the samples related to (103) phase (i.e. 63°) and (102) phase (47.69°) is 388 nm and 361 nm respectively. Except PHB-10HZ5 composite sample, all other samples in (110) phase (56.75°) was observed with the average crystallite size around 376 nm.

3.1.3 Dislocation density analysis

Dislocation is a line defect or crystallographic defect or irregularities present within the crystal structure which affects the material properties strongly. Dislocation density is a measure of number of dislocations per unit volume of crystalline material [45]. The dislocation density of

PHB-10HZ0 copolymer and ZnO NPs in the PHB-10HZ0/ZnO NPs composite was determined using the following equation

$$\text{Dislocation Density } (\delta) = 1/D^2 \quad (3)$$

and the calculated dislocation density values are plotted against different ZnO NPs concentration as shown in Fig. 10a & 10b. The calculated values lie within 10^{12} lines/m². From the Fig. 10a, it clearly shows the effect of ZnO NPs in PHB10HZ0 copolymer's dislocation density. As mentioned earlier, we eliminated PHB-10HZ20 sample's dislocation density observed at 25.61° (Fig. 10a) for the same reason mentioned in the previous paragraph. As the concentration of ZnO NPs increases, the dislocation density values are fluctuating randomly and very high δ value is observed for PHB-10HZ0, PHB-10HZ5, PHB-10HZ25 and PHB-10HZ30 samples related to (020), (040), (021) and (121) phases respectively. It is clear from the fig. 10a, on considering the phases or peaks, overall the dislocation density values of PHB-10HZ0 copolymer is high along (020) phase and then gradually decreasing for other phases in all other samples except PHB-10HZ5 along (040) phase, PHB-10HZ25 along (040) phase, PHB-10HZ25 along (021) & (121) phase and PHB-10HZ30 along (121) phase. PHB-10HZ10, PHB-10HZ15, PHB-10HZ20 exhibit high dislocation density value in (121), (020), (021) phase respectively. Fig. 10b shows the change in dislocation density of ZnO NPs in PHB-10HZ0/ZnO NPs composite with respect to different ZnO NPs concentration. It is clear from the fig. 10b that high δ value was observed only for PHB-10HZ15 sample along the (100), (002) and (101) phases. All the samples exhibit a very low and almost equal value along the (102) and (103) phases. From the observation, high value of δ could be noticed for ZnO lattice in PHB-10Z15 polymer matrix and undergoes severe structural defects whereas the higher concentration ($> 15\%$ ZnO NPs) exhibit moderate structural defects.

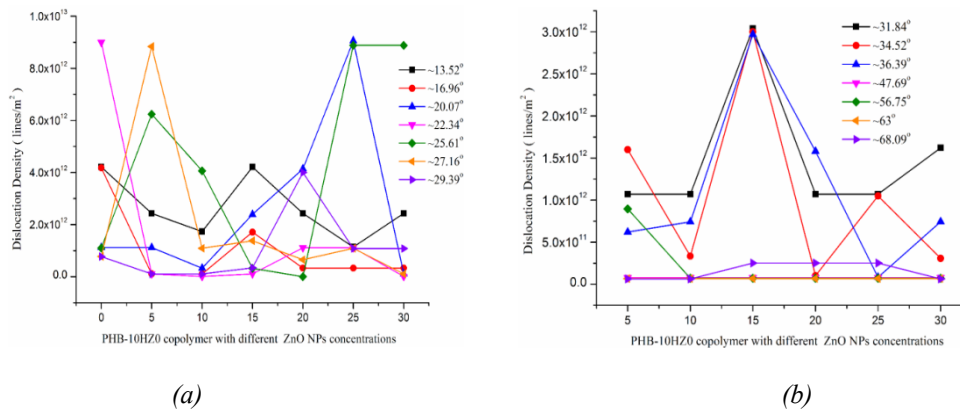


Fig. 10. a) Variation in dislocation density of PHB-10HZ0 copolymer in PHB-10HZ0/ZnO NPs composite with respect to different ZnO NPs concentrations, b) Variation in dislocation density of ZnO NPs in PHB-10HZ0/ZnO NPs composite with respect to different ZnO NPs concentrations.

3.1.4 Texture coefficient analysis

Texture is the distribution of crystallographic orientations of a polycrystalline sample. Texture coefficient was used to determine the preferred orientation of the crystal of PHB-10HZ0 copolymer and ZnO NPs, which is calculated by the following equation [46].

$$T_c(hkl) = \frac{I_a(hkl)/I_o(hkl)}{(1/N) [\sum_N I_a(hkl)/I_o(hkl)]} \quad (4)$$

where $T_c(hkl)$ is the texture coefficient of the (hkl) plane, I_a is the measured intensity, I_o is standard intensity and N is the number of diffraction peaks considered for this analysis. From the above equation, if the $T_c(hkl)$ is close to unity then the (hkl) plane is randomly distributed. If $T_c(hkl)$ is greater than 1, then the (hkl) plane is preferentially oriented for the crystal growth.

The prominent peaks such as 13.52° , 16.96° , 22.34° and 25.6° corresponding to (020), (110), (111), and (040) orientations which belongs to PHB-10HZ0 copolymer was considered in this study since the intensity of other peaks are not known. For ZnO NPs, the following peaks observed at 31.84° , 34.52° , 36.39° , 47.69° , 56.75° , 63.01° , 68.09° corresponding to (100), (002), (101), (102), (110), (103) and (112), reflections were considered in this analysis (JCPDS 790205). The change in texture coefficient of PHB-10HZ0 copolymer and ZnO NPs with respect to the above-mentioned peaks with different ZnO NPs concentrations is shown in Fig. 11a & 11b respectively.

Fig. 11a shows the texture coefficient values with respect to PHB-10HZ0 copolymer for different ZnO NPs concentrations. It is clearly evident from the fig. 11a that the preferential phase is (020) than all other phase considered in this analysis, since the observed $T_c(020)$ value of all the samples is around 2 which is greater than unity. The T_c value of (110) phase is greater than 1 for PHB-10HZ25 sample which makes it as a preferential oriented phase for that sample whereas for all other samples, the T_c value of (110) phase is less than unity (~ 0.9), which makes that as a randomly oriented phase.

The texture coefficient analysis should be addressed for ZnO NPs, since the addition of ZnO NPs in the PHB-10HZ0 copolymer matrix could leads to structural modification which ultimately influence the preferred crystal orientation. Figure 11b shows the texture coefficient values of ZnO NPs in the PHB-10HZ0 composites for different ZnO NPs concentrations. It is clearly evident from the Fig. 11b that the addition of ZnO NPs in the PHB-10HZ0 copolymer affect the preferred orientation of crystal with respect to different concentrations of ZnO NPs. For PHB-10HZ5 sample, the preferential phase is (100) and (102), since the T_c value of these mentioned phase was greater than unity whereas the T_c value of all other phase was less than unity, making these orientations as a randomly distributed orientation. The T_c value of (100), (002) and (102) is approx. 1.16, which is greater than unity that makes it as a preferentially oriented phase for PHB-10HZ10 sample. On considering the PHB-10HZ15 sample, T_c value of (100), (102) and (110) exhibited greater than unity which makes those three phases as a preferentially oriented one, whereas all other phases were random. PHB-10HZ20 sample's preferred orientations were (102) and (110), since it exhibits T_c value around ~ 1.08 . PHB-10HZ25 and PHB-10HZ30 has four preferred orientations. Both the samples have three same preferred orientation such as (100), (102), and (110) orientations, whereas the fourth orientation is different. The fourth preferred orientation for PHB-10HZ25 and PHB-10HZ30 sample was (101) and (002) respectively.

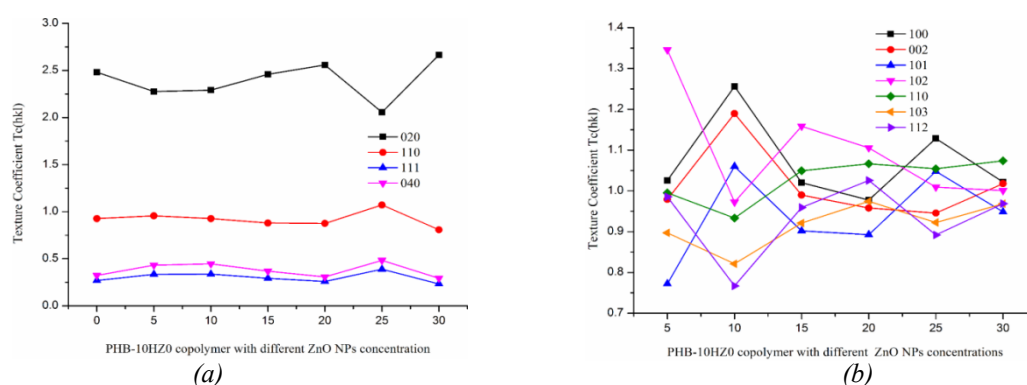


Fig. 11. a) Change in texture coefficient of PHB-10HZ0 copolymer in PHB-10HZ0/ZnO NPs composite with respect to different ZnO NPs concentrations, b) change in texture coefficient of ZnO NPs in PHB-10HZ0/ZnO NPs composite with respect to different ZnO NPs concentrations.

The T_c values of peak 31.84° indexed as (100) is greater than unity for all the samples except PHB-10HZ20 which makes that as a preferentially oriented phase for all the samples except PHB-10HZ20. From the Fig. 11b, T_c value of (002) oriented phase exhibits greater than one only for PHB-10HZ10 and PHB-15HZ30 which makes it as a prominent orientation and reveals the

support of ZnO NPs on the structural modification, whereas T_c value of (101) oriented phase is greater than one for PHB-10HZ10 and PHB-10HZ25. T_c of the peak observed at 47.69° indexed to (102) orientation is greater than unity for all the samples except PHB-10HZ10 sample whereas the T_c of (110) orientation is greater than unity for the samples which contains ZnO NPs greater than or equal to 15 percent. (103) orientation is the only random orientated phase for all the samples since it exhibited T_c value less than unity. The T_c of (112) orientation is exactly opposite to that of (100) orientation.

Overall, from the XRD analysis, reinforcement of ZnO NPs in the PHB-10HZ0 copolymer suppresses the crystalline behaviour for all the samples except PHB-10HZ20 which shows high crystallinity than virgin PHB-10HZ0 copolymer along the preferred orientation or peaks of PHB-10HZ0 copolymer. In addition to that, with respect to the concentration of PHB-10HZ0 copolymer in the PHB-10HZ0/ZnO NPs composites, there is some crystal defects and structural modification in the ZnO lattice that changes the intensity of ZnO NPs peaks. However, the intensity of ZnO NPs peaks dominates the PHB-10HZ0 copolymer peaks.

3.2 Optical characterization

3.2.1 Absorption and reflectance spectra

In order to analyse the effect of ZnO NPs on the optical properties of PHB-10HZ0 copolymer, the absorption, reflectance and transmittance spectra was captured and plotted in a graph as shown in Fig. 12a & 12b respectively. Figure 12a clearly shows that the all samples show good absorption peak intensity (~ 11 a.u.) around 200 nm (UV-C region), then gradually decreases and reached around ~ 6 a.u. for 250- 320 nm (UV-B region). It is clearly evident from the Fig. 12a that the absorption rate is gradually decreasing as the wavelength increases with a very low value observed (~ 2.5 a.u.) in the wavelength range from 800 to 1000 nm.

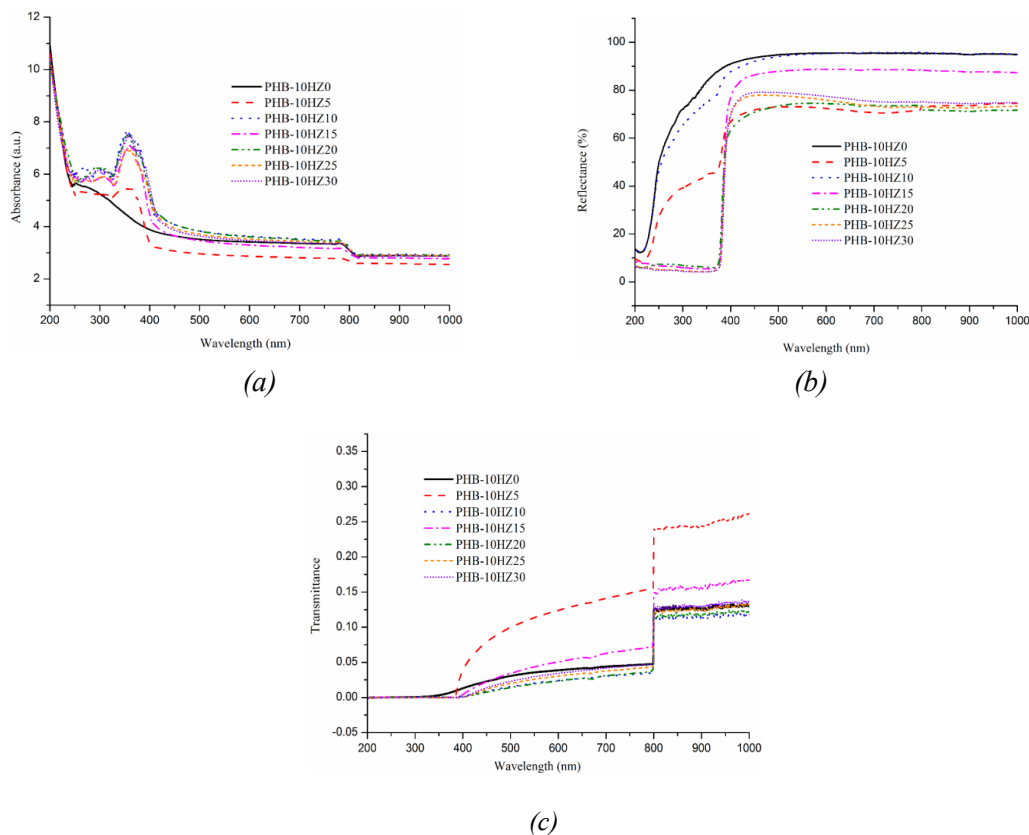


Fig. 12. a) Absorbance, b) reflectance and c) transmittance spectra of virgin PHB-10HZ0 copolymer and ZnO NPs reinforced PHB-10HZ0 composites

Apart from that, there are two distinct absorption peaks could be observed in the wavelength range from 250 to 310nm (UV-B region) and from 350 nm to 360 nm in which a strong absorption peak is located in between 350nm and 360 nm (UV-A region) and attributed to the typical exciton absorption peak (355nm) of ZnO NPs at room temperature [47, 28]. It is evident from the Fig. 12a that the significant sharp absorption peak of ZnO indicates the monodispersed nature of nanoparticle [48]. Figure 12a clearly shows that the absorption edge systematically shifts to lower wavelength or higher energy with the decreasing concentration of the nanoparticles. Quantum size effect is an evident for these kind of observation [49]. Fig. 12a also depicts that, compared to virgin PHB-10HZ0 copolymer the absorbance spectra intensity shows high value at ~355 nm (UV-A region) for PHB-10HZ5 sample and gradually increases with the increasing concentration of ZnO NPs. The absorbance of virgin PHB-10HZ0 copolymer sample is high around ~200 nm and gradually decreases with increase in wavelength with no excitation peak around ~355nm. Overall the ZnO reinforced PHB-10HZ0 samples shows a very good absorption value in the UV region i.e. from 200nm to 400nm. Fig. 12a clearly shows a drop in the absorbance curve at ~754 nm (visible region) for all the samples which clearly indicates that the sample has very low absorption in the visible region.

The reflectance spectra of virgin PHB-10HZ0 copolymer and ZnO NPs reinforced PHB-10HZ0 composites are shown in fig. 12b. It is clear from fig. 12b that PHB-10HZ0/ZnO NPs composites exhibit low reflection (5% to 9%) in UV region and high reflection (70% to 88%) in visible region whereas virgin PHB-10HZ0 attain high reflection (> 70%) in almost all the measured wavelength.

3.2.2 Transmittance spectra

In order to further investigate the absorption results, transmittance behavior of virgin PHB-10HZ0 copolymer and ZnO NPs reinforced PHB-10HZ0 samples were analyzed and the obtained data were plotted as shown in Fig. 12c. It is clearly evident from the fig. 12c, the transmittance value of all the composites are almost zero in the wavelength range of 200-400nm. For the virgin PHB-10HZ0 copolymer, the transmittance value is almost zero in the wavelength range from 200nm to 320 nm and then gradually increases with the increase in the wavelength. Skin cancer, sun burn, damage to the eye tissues and plastic degradation is caused by the increased UV-B radiation exposure (290 to 315 nm) [50]. From these observation, it is suggested to use the PHB-10HZ0/ZnO NPs composite as a UV blocker or absorber.

3.3 Surface analysis

The surface of the casted films should be investigated since any changes in the structural parameters may impact the surface morphology of the casted film samples. In order to investigate the effect of ZnO NPs in the surface morphology, virgin PHB-10HZ0 copolymer and ZnO NPs reinforced PHB-10HZ0 composite film samples were analyzed by using Atomic Force Microscopy and 3D images of all the film samples were taken as shown in Fig. 13.

Table 2. Surface parameters of virgin PHB-10HZ0 copolymer and ZnO NPs/ PHB-10HZ0 composite samples.

Sample Name	Roughness (μm)	Particle size Density ($/\mu\text{m}^2$)	Particle size Diameter (μm)
PHB-10HZ0	0.24	0.018	0.949
PHB-10HZ5	0.184	0.062	1.198
PHB-10HZ10	0.212	0.03	1.073
PHB-10HZ15	0.0519	0.085	0.857
PHB-10HZ20	0.585	0.21	0.873
PHB-10HZ25	0.217	0.049	1.176
PHB-10HZ30	0.302	0.025	1.961

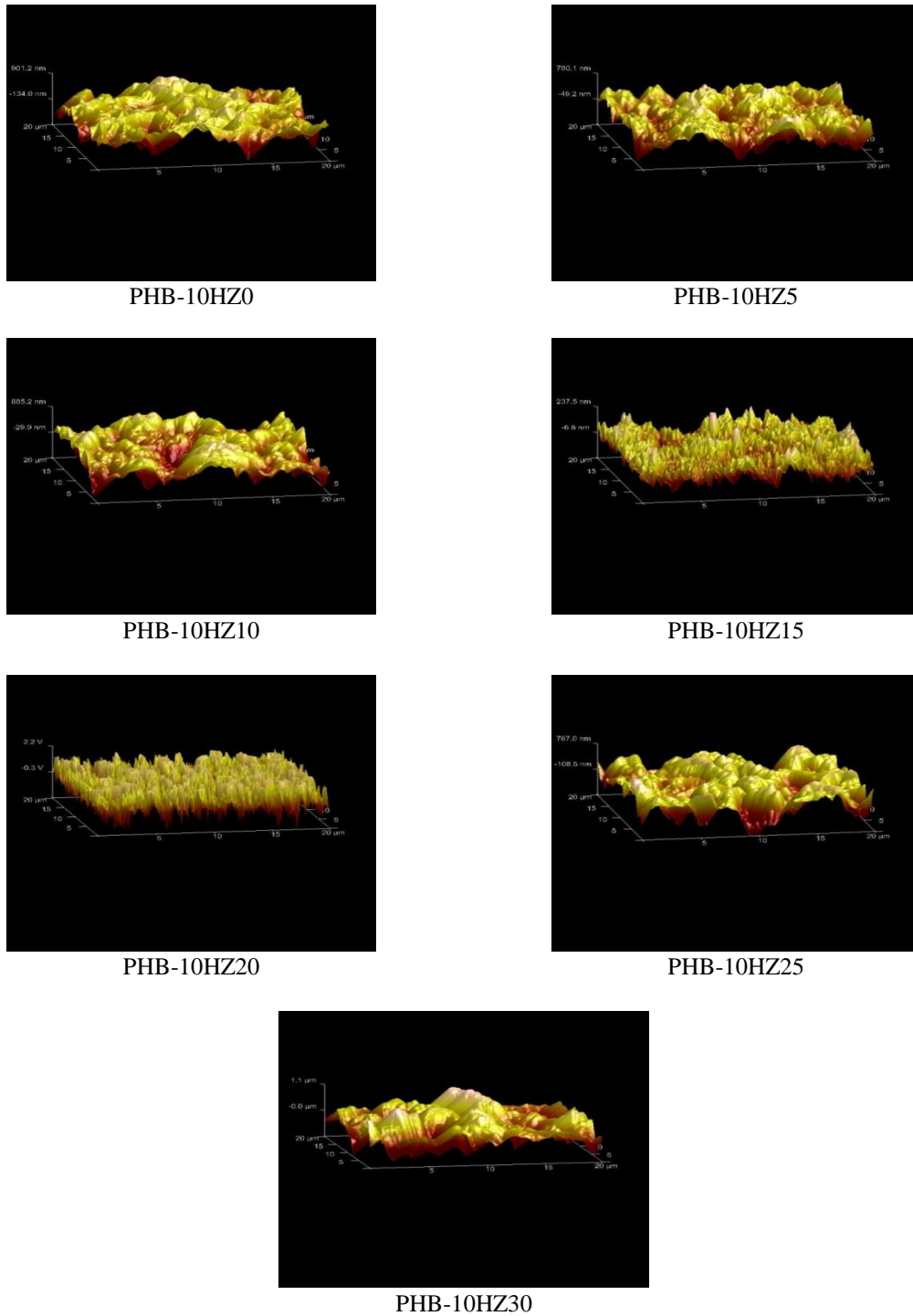


Fig. 13. AFM surface images of virgin PHB-10HZ0 copolymer and ZnO NPs reinforced PHB-10HZ0 composites.

Fig. 13 shows the influence of ZnO NPs in the surface morphology of PHB-10HZ0 copolymer. The structural changes are clearly visible in all the samples from the fig. 13 and to analyze further, nanoscope analysis software is used to determine the structural parameters such as roughness, surface density and particle size of Virgin PHB-10HZ0 and ZnO mixed PHB-10HZ0 composite film samples and the obtained data's are enumerated in table – 2. From the table - 2, virgin PHB-10HZ0 copolymer film sample shows roughness value around $\sim 0.240\mu\text{m}$ and then gradually decreases to very low roughness value ($0.052\mu\text{m}$) encountered for PHB-10HZ15

composite sample and then increases to (0.302 μm) for PHB-10HZ25 composite sample. Overall the roughness of the sample increases as the concentration of ZnO NPs increases in the PHB-10HZ0 copolymer. It may be due to the effect of surface level agglomeration of ZnO NPs. Particle size also follows the same trend as very low value (0.857 μm) observed for PHB-10HZ15 samples. Overall the particle size increases with increase in ZnO NPs concentration. Virgin PHB-10HZ0 copolymer has very low surface density compared to the ZnO NPs reinforced PHB-10HZ0 copolymer.

4. Conclusions

This study investigates the structural and optical properties of virgin P(3HB-*co*-10 mol% 3HHx) copolymer and ZnO NPs reinforced P(3HB-*co*-10 mol% 3HHx) composite films which was fabricated by solution casting method. ZnO NPs acts as a retarding agent which decreased the crystallinity except for 20% ZnO concentration whereas it increased the dislocation density with respect to the orientation of P(3HB-*co*-10 mol% 3HHx) copolymer. Texture coefficient analysis revealed that P(3HB-*co*-10 mol% 3HHx) copolymer and its composites had preferential orientation of (020) than all other orientations. Addition of ZnO NPs increased the absorption behaviour in UV region and decreased the absorption in visible region which was studied by UV-Vis spectroscopy. Overall the prepared ZnO NPs reinforced P(3HB-*co*-10 mol% 3HHx) composites may be used as UV-blocker or mask coating in printed circuit board, however the in depth analysis on UV-curing and degradation studies is still needed to develop a prototype product.

Acknowledgement

Author expresses gratitude to USM Fellowship for financial support, Dr. Sudesh Kumar and Murugan Paramasivan from Ecobiomaterial Research Laboratory, School of Biological Sciences, Universiti Sains Malaysia Main campus for providing the biopolymer material and Dr. Shahrom Mahmud for providing the ZnO nanoparticles for our experimental work.

References

- [1] M. Duncan, *Journal of Industrial Ecology* **7**(3-4), 193(2003).
- [2] M. D. Sanchez-Garcia, E. Gimenez, J. M. Lagaron, *Carbohydrate Polymers* **71**(2), 235(2008).
- [3] C. S. K. Reddy, R. Ghai, V. Kalia, *Bioresource Technology* **87**(2), 137 (2003).
- [4] J. Aguado, D. P. Serrano, "Feedstock recycling of plastic wastes (Vol. 1)", Royal society of chemistry, 1999.
- [5] A. Azapagic, A. Emsley, I. Hamerton, "Polymers: the environment and sustainable development", John Wiley & Sons, 2003.
- [6] A. Fletcher, "PHA as natural, biodegradable polyesters' in *Plastics from Bacteria and for Bacteria* " Springer-Verlag, New York, 77, 1993.
- [7] R. M. Atlas, "Microbial Ecology: Fundamentals and Applications", third ed., 39 1993.
- [8] S. Song, S. Hein, A. Steinbüchel, *Biotechnology Letters*, **21**(3), 193 (1999).
- [9] C. R. Alvarez-Chavez, S. Edwards, R. Moure-Eraso, K. Geiser, *Journal of Cleaner Production*, **23**(1), 47 (2012).
- [10] M. A. Abdelwahab, A. Flynn, B. S. Chiou, S. Imam, W. Orts, E. Chiellini, *Polymer Degradation and Stability* **97**(9), 1822 (2012).
- [11] M. Avella, J. J. De Vlieger, M. E. Errico, S. Fischer, P. Vacca, M. G. Volpe, *Food Chemistry* **93**(3), 467 (2005).
- [12] S. Khanna, A. K. Srivastava, *Process Biochemistry* **40**(2), 607 (2005).

- [13] A. Steinbüchel, B. Fuchtenbusch, *Trends in Biotechnology* **16**(10), 419 (1998).
- [14] C. S. Wu, *Journal of Applied Polymer Science* **102**(4), 3565 (2006).
- [15] A. J. Anderson, E. A. Dawes, *Microbiological Reviews* **54**(4), 450 (1990).
- [16] G. J. Griffin, "Chemistry and technology of biodegradable polymers", Blackie academic & professional, 1994.
- [17] N. Galego, C. Rozsa, R. Sanchez, J. Fung, A. Vazquez, J. Santo Tomas, *Polymer Testing*, **19**(5), 485 (2000).
- [18] C. Doyle, E. T. Tanner, W. Bonfield, *Biomaterials* **12**(9), 841 (1991).
- [19] R. Jain, S. Kosta, A. Tiwari, *Chronicles of Young Scientists* **1**(3), 10 (2010).
- [20] S. S. Ray, M. Bousmina, *Progress in Materials Science* **50**(8), 962 (2005).
- [21] P. Kahar, T. Tsuge, K. Taguchi, Y. Doi, *Polymer Degradation and Stability* **83**(1), 79 (2004).
- [22] T. G. Volova, "Polyhydroxyalkanoates--plastic materials of the 21st century: production, properties, applications", Nova publishers, 2004.
- [23] E. P. Giannelis, *Advanced Materials* **8**(1), 29 (1996).
- [24] M. Sadat-Shojai, M. T. Khorasani, A. Jamshidi, S. Irani, *Materials Science and Engineering: C* **33**(5), 2776 (2013).
- [25] M. Erceg, T. Kovacic, I. Klaric, "Kinetic analysis of the isothermal degradation of PHB/OMMT nanocomposites", In Fourth International Symposium on Nanostructured and Functional Polymer-based Materials and Nanocomposites, January, 2008.
- [26] C. Xu, Z. Qiu, *Polymers for Advanced Technologies* **22**(5), 538 (2011).
- [27] A. M. Nafchi, R. Nassiri, S. Sheibani, F. Ariffin, A. A. Karim, *Carbohydrate Polymers* **96**(1), 233 (2013).
- [28] S. Talam, S. R. Karumuri, N. Gunnam, International Scholarly Research Network. ISRN Nanotechnology, 2012, Article ID 372505.
- [29] M. A. Mitchnick, D. Fairhurst, S. R. Pinnell, *Journal of the American Academy of Dermatology* **40**(1), 85 (1999).
- [30] W. Yu, C. H. Lan, S. J. Wang, P. F. Fang, Y. M. Sun, *Polymer* **51**(11), 2403 (2010).
- [31] A. M. Diez-Pascual, A. L. Diez-Vicente, *International Journal of Molecular Sciences* **15**(6), 10950 (2014).
- [32] A. B. Devi, C. V. Nachiyar, T. Kaviyarasi, A. V. Samrot, *International Journal of Pharmacy and Pharmaceutical Sciences* **7**(3), 140 (2015).
- [33] C. P. Liao, M. Bin Ahmad, K. Shameli, W. M. Z. W. Yunus, N. A. Ibrahim, N. Zainuddin, Y. Y. Then, *The Scientific World Journal* **2014**, (2014).
- [34] F. C. Oliveira, M. L. Dias, L. R. Castilho, D. M. Freire, *Bioresource Technology* **98**(3), 633 (2007).
- [35] A. M. Nair, K. Annamalai, S. K. Kannan, S. Kuppusamy, *Malaya J. Biosci.* **1**, 8 (2014).
- [36] C. Chen, P. H. Yu, M. K. Cheung, *Journal of Applied Polymer Science* **98**(2), 736 (2005).
- [37] S. Nakamura, Y. Doi, M. Scandola, *Macromolecules* **25**(17), 4237 (1992).
- [38] V. Sridhar, I. Lee, H. H. Chun, H. Park, *Express Polymer Letters* **7**(4), 320 (2013).
- [39] R. M. D. S. M. Thiré, L. C. Arruda, L. S. Barreto, *Materials Research* **14**(3), 340 (2011).
- [40] J. J. Song, S. C. Yoon, M. Y. Seungju, R. W. Lenz, *International Journal of Biological Macromolecules* **23**(3), 165 (1998).
- [41] N. B. Rithin Kumar, V. Crasta, R. F. Bhajantri, B. M. Praveen, *Journal of Polymers* **2014**, (2014).
- [42] W. Guo, J. Duan, W. Geng, J. Feng, S. Wang, C. Song, *Microbiological Research* **168**(4), 231 (2013).
- [43] J. D. Makinson, J. S. Lee, S. H. Magner, R. J. De Angelis, W. N. Weins **42**, 407 (2000).
- [44] F. A. El-Kader, N. A. Hakeem, I. S. Elashmawi, A. M. Ismail, *Australian Journal of Basic and Applied Sciences* **7**(10), 608 (2013).
- [45] <http://www.virginia.edu/bohr/mse209/chapter7.htm> (Accessed 10 June 2018).
- [46] J. A. R. Marquez, C. M. B. Rodriguez, C. M. Herrera, E. R. Rosas, O. Z. Angel, O. T. Pozos, *Int. J. Electrochem. Sci.* **6**(9), 4059 (2011).
- [47] Y. D. Jin, J. P. Yang, P. L. Heremans, M. Van der Auweraer, E. Rousseau, H. J. Geise, G. Borghs, *Chemical Physics Letters* **320**(5), 387 (2000).
- [48] D. H. Zhang, Z. Y. Xue, Q. P. Wang, *Journal of Physics D* **35**(21), 2837 (2002).

- [49] M. S. Samuel, L. Bose, K. C. George, *Academic Review* **16**(1-2), 57 (2009).
- [50] A. Hanslmeier, "Space Weather and Radiation Damage. In *The Sun and Space Weather*", Springer Netherlands, 175, 2007.